Characterizing the Gate-to-Source Nonlinear Capacitor Role on GaAs FET IMD Performance

José Angel García, *Student Member, IEEE*, Angel Mediavilla Sánchez, *Member, IEEE*, José Carlos Pedro, *Member, IEEE*, Nuno Borges de Carvalho, *Student Member, IEEE*, Antonio Tazón Puente, *Member, IEEE*, and José Luis García, *Member, IEEE*

***Abstract*— This paper discusses, in a mathematical form and supported by a complete special experimental characterization, the gate-to-source nonlinear capacitor contribution on small-signal intermodulation distortion (IMD) as well as other nonlinear related phenomena such as the onset of phase distortion and gain compression in GaAs FET devices. A simplified one-sided version of our previously proposed test setup and its corresponding characterization formulation are shown to conform a direct and trustful technique to extract the second- and third-order coefficients for the $Cgs(Vgs)$ Taylor-series expansion. The extracted terms let us evaluate some of the most widely employed equations for this reactive nonlinearity according to their capability of reproducing its small-signal nonlinear distortion contribution. They are also shown to be responsible for some previously detected differences on IMD behavior at high frequencies and for significant variations on the load selection criteria for high carrier-to-intermodulation ratio and high output-power tradeoffs.**

***Index Terms*— Intermodulation distortion, MESFET's, microwave measurements, modeling, Volterra series.**

I. Introduction

THE nonlinear distortion prediction in microwave circuits is still an important open field in today's research efforts. The modern wireless communications systems require the development of new simulation techniques, such as spectral balance and envelope-transient analysis, for handling a large number of noncommensurate tones, as well as an accurate characterization of the most employed nonlinear devices for these purposes. This second element is the one discussed in this paper.

It has been accepted as a law in [1] that reproducing the small-signal second- and third-order intermodulation distortion (IMD) and the related phenomena—AM/PM conversion, gain compression, etc.—on a nonlinear device is only possible if its model not only accurately describes the nonlinear current/voltage I/V and charge/voltage Q/V characteristics, but also their respective derivatives at least up to the same order. As a mild nonlinear device, either successive numeric differentiations or least-squares fittings of the commonly measured characteristics for an FET have been proven to be inadequate for extracting these derivatives [2]. Maas *et al.* gave the first solution to this problem in [2] and [3] for the predominant nonlinearity $Ids(Vgs)$ with a direct and very simple technique based on harmonic measurements at the drain side. That effective procedure was later extended in [4] for the complete bi-dimensional $Ids(Vgs, Vds)$ Taylor-series expansion. The reported experimental extractions, still scarce, have permitted evaluation of the Ids equations for IMD purposes since then, and have lead to important conclusions on bias and load control for low nonlinear distortion designs. The reactive nonlinearities have been considered of secondary or minor effect; however, not disposing of an experimental procedure for extracting their power-series terms has determined the current incapacity for evaluating the extent of its minor role as it has been recently considered [5].

In this paper, we intend to show the accurate role $Cgs(Vgs)$ nonlinear capacitor plays on IMD performance and phase-distortion onset for applications in the saturated region. This will be accomplished by extracting its second- and third-order Taylor-series coefficients versus the gate-to-source bias voltage $Vgso$ through a simplified procedure of the one recently proposed in [6] for the complete bi-dimensional $Qg(Vgs, Vgd)$ expansion. The modified test setup, its corresponding direct formulation, and the solution to the detected problems in [7] for the region where $Cgs(Vgs)$ relative importance could be small, conforms a trustful technique for getting its second- and third-order derivatives. It also allows the analysis of its responsibility, along with $Ids(Vgs, Vds)$, in the IMD performance versus bias and load impedance at high frequencies, something experimentally reported in previous significant works such as [8] for gate mixers and [9] for amplifiers.

Some of the currently most employed $Cgs(Vgs)$ equations are analyzed for the first time according to their second- and third-order derivatives behavior and their resulting IMD prediction. The output power and carrier-to-intermodulation (C/I) ratio load–pull contours, which are so widely employed for designing low-distortion amplifiers, are obtained for both Cgs linear and nonlinear, supporting significant differences

Manuscript received April 3, 1998; revised September 1, 1998. This work was supported in part by the Agencia Española de Cooperación Internacional under an MUTIS Grant, and in part by the 35/98 Spanish–Portuguese Integrated Research Action.

J. A. García, A. Mediavilla Sánchez, A. Tazón Puente, and J. L. García are with the Department Ingenieria de Comunicaciones, Universidad de Cantabria, 39005 Santander, Spain.

J. C. Pedro and N. B. de Carvalho are with the Instituto de Telecomunicações, Universidade de Aveiro, 3810 Aveiro, Portugal.

Publisher Item Identifier S 0018-9480(98)09198-4.

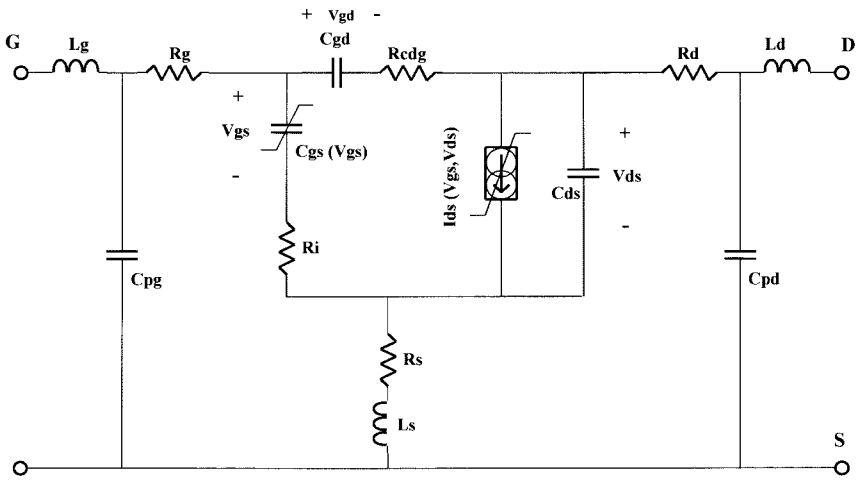

Fig. 1. MESFET nonlinear equivalent circuit.

in the optimum-load-condition selection due to the $Cgs(Vgs)$ contribution now available.

Gain compression and phase-distortion contours give us some further insight into the reactive derivatives nonlinear distortion role, and could confirm, in a mathematical way (just for the small-signal regime where third-order Volterra analysis is valid), previously published experimental results [10]. However, large-signal multitone behavior, also experimentally reported in [9] and [10], would require an adequate analysis tool for evaluating the $Cgs(Vgs)$ role on IMD.

II. Mathematical Formulation and Experimental Setup

It is well known that the nonlinear currents technique for Volterra-series analysis ([11], [12]) is a simple and powerful tool for small-signal nonlinear distortion calculations. We have used this methodology for extracting the $Cgs(Vgs)$ Taylor-series coefficients, just as it was employed for the Ids derivatives extraction [2]–[4]. We consider the widely accepted equivalent circuit of Fig. 1 for an FET, where $Cgs(Vgd)$ dependence is not taken into account, and Cgd is assumed linear, a common practice for applications in the saturated region. The mathematical formulation considers the complete $Ids(Vgs, Vds)$ nonlinearity due to the important contribution of its cross terms on the IMD predictions with load condition control, although we will also show the possibility of approximately extracting the reactive derivatives for a simplified transconductance description of $Ids(Vgs)$.

The complete Taylor-series expansion up to third order for $Qg(Vgs, Vgd)$ in

$$\begin{aligned} Qg(Vgs,Vgd) = {} & Qg(Vgso,Vgdo) + Cgs1 \cdot vgs + Cgd \\ & \cdot vgd + Cgs2 \cdot vgs^2 + Cgsgd \cdot vgs \cdot vgd \\ & + Cgd2 \cdot vgd^2 + Cgs3 \cdot vgs^3 + Cgs2gd \\ & \cdot vgs^2 \cdot vgd + Cgsgd2 \cdot vgs \cdot vgd^2 \\ & + Cgd3 \cdot vgd^3 \end{aligned} \tag{1a}$$

would result in the simplified (1b), under the mentioned assumptions

$$\begin{aligned} Qg(Vgs,Vgd) = {} & Qg(Vgso,Vgdo) + Cgs1 \cdot vgs + Cgd \\ & \cdot vgd + Cgs2 \cdot vgs^2 + Cgs3 \cdot vgs^3 \end{aligned} \tag{1b}$$

Accordingly, the $Cgs(Vgs)$ and $Ids(Vgs, Vds)$ expansions are as follows:

$$Cgs(Vgs) = Cgs1 + 2 \cdot Cgs2 \cdot vgs + 3 \cdot Cgs3 \cdot vgs^2 \tag{2}$$

and

$$\begin{aligned} Ids(Vgs,Vds) = {} & Ids(Vgso,Vdso) + Gm1 \cdot vgs \\ & + Gds \cdot vds + Gm2 \cdot vgs^2 + Gmd \\ & \cdot vgs \cdot vds + Gd2 \cdot vds^2 + Gm3 \\ & \cdot vgs^3 + Gm2d \cdot vgs^2 \cdot vds \\ & + Gmd2 \cdot vgs \cdot vds^2 + Gd3 \cdot vds^3. \end{aligned} \tag{3}$$

$Qg(Vgso, Vgdo)$ and $Ids(Vgso, Vdso)$ represent the static dc values at the bias control voltages $Vgso$, $Vgdo$, and $Vdso$. The upper cases Qg, Ids, Vgs, Vgd, and Vds are the total magnitudes and the lower cases their corresponding time-varying components. Finally, the G's and C's are the respective resistive and reactive coefficients associated to the derivatives, as in [4] and [6].

In Fig. 2, we present a block diagram of the test setup we propose for the $Cgs(Vgs)$ derivatives characterization. It is a simplified version of the one proposed in [6], and a complement of the one Maas suggested in [2] and [3] for the transconductance derivatives extraction. We measure second- and third-order harmonic power levels for a sinusoidal excitation with amplitude high enough to produce levels over the spectrum-analyzer noise floor, but within the small-signal regime where Volterra-series analysis is valid. There have to be two distinguishing differences from Maas setup if we want to extract terms of an input reactive nonlinearity: first, we have to measure the harmonic power levels in gate instead of drain because the relative contribution of the predominant nonlinearity Ids is much lower there, not hiding Cgs effects; and second, we have to increase the excitation frequency up to about 1 GHz to make Cgs nonlinearity generate measurable harmonic power levels in GaAs FET devices.

The second- and third-order harmonic amplified power levels are referred to the first harmonic (fundamental) reflected power level measured via the directional coupler in order to

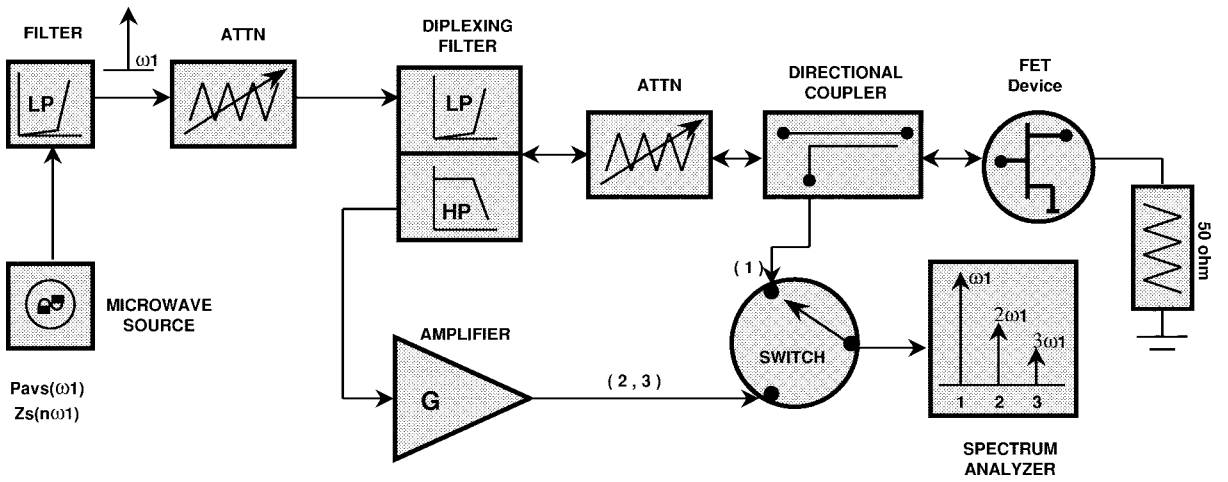

Fig. 2. Test setup for $Cgs(Vgs)$ nonlinear characterization.

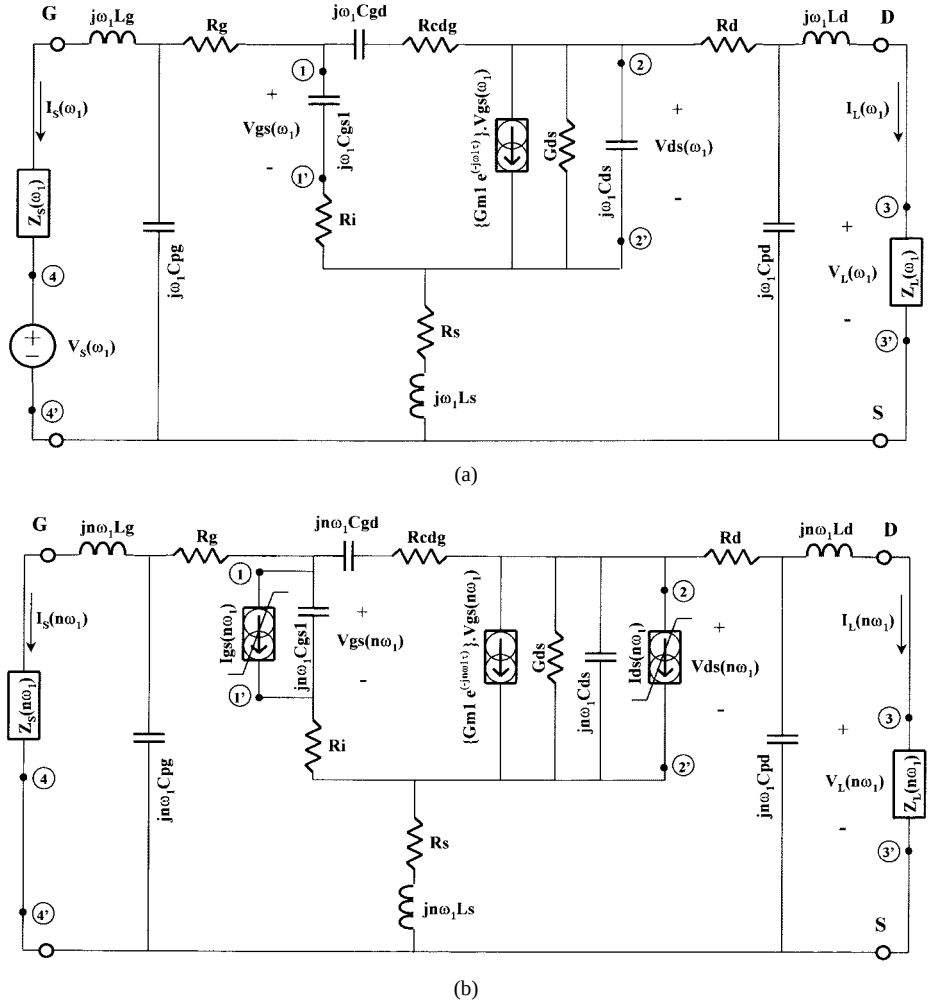

Fig. 3. Nonlinear currents topologies. (a) First-order circuit. (b) High-order circuits.

define two IMD ratios (4) and (5) reducing the spectrum-analyzer absolute-power-level error as follows:

$$IMRmeas(2\omega 1) = \frac{Ps(2\omega 1)}{Ps(\omega 1)} \tag{4}$$

$$IMRmeas(3\omega 1) = \frac{Ps(3\omega 1)}{Ps(\omega 1)} \tag{5}$$

With an adequate calibration technique, based on the test setup characterization, these measured ratios ($IMRmeas$) can be easily related to the "corrected" ratios IMR. These corrected ratios relate the powers, dissipated by the corresponding harmonic and fundamental, in the Thévenin equivalent generator resistance at the device terminals [Zs in Fig. 3(a) and (b)].

The circuit solution through the nonlinear currents technique is obtained from successive analysis of linear circuits, one for each order up to the one of our interest. These linear topologies are shown in Fig. 3(a) and (b) for the first and higher orders, respectively. We have placed ports 1 and 2 at the nonlinearities and ports 3 and 4 at the load and generator in respective order. Although port 3 is not necessary for the extraction procedure, it will be useful for later IMD calculations. The linear elements in the transistor equivalent circuit, as well as the generator and load impedances, are included in the four-port linear associated circuit, as in [12]. The capacitors in Fig. 3(a) and (b) have been represented by their susceptance, while the inductors by their reactance.

The Y matrix equation results in

$$-\begin{bmatrix} Igs \\ Ids \\ 0 \\ Is \end{bmatrix} = \begin{bmatrix} Y_{11} & Y_{12} & Y_{13}Y_{14} \\ Y_{21} & Y_{22} & Y_{23}Y_{24} \\ Y_{31} & Y_{32} & Y_{33}Y_{34} \\ Y_{41} & Y_{42} & Y_{43}Y_{44} \end{bmatrix} \times \begin{bmatrix} Vgs \\ Vds \\ Vl \\ Vs \end{bmatrix} \tag{6}$$

where Igs and Ids represent the nonlinear current sources for $Cgs(Vgs)$ and $Ids(Vgs, Vds)$ nonlinearities, respectively. $Il = 0$ for every order since ZL was included in the linear associated circuit.

With the previously corrected ratios IMR and the equivalent generator available power $Pavs(\omega 1)$, we can determine the magnitudes of the second- and third-order nonlinear transfer functions $H2(\omega 1, \omega 1)$ and $H3(\omega 1, \omega 1, \omega 1)$, relating the phasors $Is(2\omega 1)$ and $Is(3\omega 1)$ in Fig. 3(b) for the second- and third-order harmonic components of the gate current to the excitation phasor $Vs(\omega 1)$ in Fig. 3(a) as follows:

$$|H_2(\omega 1, \omega 1)| = \frac{|Is(2\omega 1)|}{\frac{|Vs(\omega 1)|^2}{2}} = |Yin(\omega 1)| \cdot \sqrt{\frac{IMR(2\omega 1)}{2 \cdot Pavs(\omega 1) \cdot \mathrm{Re}\{Zs(2\omega 1)\}}} \tag{7}$$

$$|H_3(\omega 1, \omega 1, \omega 1)| = \frac{|Is(3\omega 1)|}{\frac{|Vs(\omega 1)|^3}{4}} = \frac{|Yin(\omega 1)|}{2 \cdot Pavs(\omega 1)} \cdot \sqrt{\frac{IMR(3\omega 1)}{\mathrm{Re}\{Zs(\omega 1)\} \cdot \mathrm{Re}\{Zs(3\omega 1)\}}}. \tag{8}$$

The second- and third-order nonlinear transfer functions are easily related to the second- and third-order coefficients of both nonlinearities once we have successively analyzed the first-, second-, and third-order associated linear circuits. We can then extract $Cgs2$ once we know $Gm2$, Gmd, and $Gd2$ (or simply the equivalent $G2$ for Maas extraction, see Appendix), as we show in (9)

$$Cgs2 = \frac{\{|H_2(\omega 1, \omega 1)| \angle \alpha_2(\omega 1, \omega 1) - K_{Isds}(2\omega 1) \cdot Hds_2(\omega 1, \omega 1)\}}{j \cdot 2 \cdot \omega 1 \cdot K_{Isgs}(2\omega 1) \cdot K^2_{Vgs}(\omega 1)} \tag{9}$$

where $\alpha_2(\omega 1, \omega 1)$ is the unknown phase of $H_2(\omega 1, \omega 1)$, and $Hds_2(\omega 1, \omega 1)$ is the nonlinear transfer function relating the phasor $Ids(2\omega 1)$ of the nonlinear current source to the corresponding excitation

$$Hds_2(\omega 1, \omega 1) = \frac{Ids(2\omega 1)}{\frac{Vs^2(\omega 1)}{2}} = K^2_{Vgs}(\omega 1) \cdot Gm2 \cdot K_{Vgs}(\omega 1) \cdot K_{Vds}(\omega 1) \cdot Gmd + K^2_{Vds}(\omega 1) \cdot Gd2. \tag{10}$$

$KVgs(\omega 1)$ and $KVds(\omega 1)$ come from the first-order equivalent circuit applying linear-circuit analysis techniques

$$\begin{bmatrix} K_{Vgs}(\omega 1) \\ K_{Vds}(\omega 1) \\ K_{Vl}(\omega 1) \end{bmatrix} = \begin{bmatrix} \frac{Vgs(\omega 1)}{Vs(\omega 1)} \\ \frac{Vds(\omega 1)}{Vs(\omega 1)} \\ \frac{Vl(\omega 1)}{Vs(\omega 1)} \end{bmatrix} = -\begin{bmatrix} Y_{11}(\omega 1) & Y_{12}(\omega 1) & Y_{13}(\omega 1) \\ Y_{21}(\omega 1) & Y_{22}(\omega 1) & Y_{23}(\omega 1) \\ Y_{31}(\omega 1) & Y_{32}(\omega 1) & Y_{33}(\omega 1) \end{bmatrix}^{-1} \times \begin{bmatrix} Y_{14}(\omega 1) \\ Y_{24}(\omega 1) \\ Y_{34}(\omega 1) \end{bmatrix} \tag{11}$$

while $KIsgs(2\omega 1)$ and $KIsds(2\omega 1)$ can be calculated for the second-order circuit

$$\begin{bmatrix} K_{Isgs}(n\omega 1) \\ K_{Isds}(n\omega 1) \\ K_{Isl}(n\omega 1) \end{bmatrix} = \begin{bmatrix} \left.\frac{Is(n\omega 1)}{Igs(n\omega 1)}\right|_{Ids(n\omega 1)=0} \\ \left.\frac{Is(n\omega 1)}{Ids(n\omega 1)}\right|_{Igs(n\omega 1)=0} \\ K_{Isl}(n\omega 1) \end{bmatrix} = \left(\begin{bmatrix} Y_{41}(n\omega 1) & Y_{42}(n\omega 1) & Y_{43}(n\omega 1) \end{bmatrix} \times \begin{bmatrix} Y_{11}(n\omega 1) & Y_{12}(n\omega 1) & Y_{13}(n\omega 1) \\ Y_{21}(n\omega 1) & Y_{22}(n\omega 1) & Y_{23}(n\omega 1) \\ Y_{31}(n\omega 1) & Y_{32}(n\omega 1) & Y_{33}(n\omega 1) \end{bmatrix}^{-1} \right)^T \tag{12}$$

with $n = 2$.

In an analogous way, $Cgs3$ can be determined with the previous knowledge of $Gm3$, $Gm2d$, $Gmd2$, and $Gd3$ (or $G3$ for the transconductance characterization, see Appendix) and both the second-order resistive and reactive coefficients

$$Cgs3 = \frac{\left\{ \begin{array}{l} |H_3(\omega 1, \omega 1, \omega 1)| \angle \alpha_3(\omega 1, \omega 1, \omega 1) \\ \quad - K_{Isds}(3\omega 1) \cdot Hds_3(\omega 1, \omega 1, \omega 1) \\ \quad - K_{Isgs}(3\omega 1) \cdot [Hgs_{3b}(\omega 1, \omega 1, \omega 1) \\ \qquad + Hgs_{3c}(\omega 1, \omega 1, \omega 1)] \end{array} \right\}}{j \cdot 3 \cdot \omega 1 \cdot K_{Isgs}(3\omega 1) \cdot K^3_{Vgs}(\omega 1)} \tag{13}$$

where $\alpha_3(\omega 1, \omega 1, \omega 1)$ is the unknown phase of $H_3(\omega 1, \omega 1, \omega 1)$, and $Hds_3(\omega 1, \omega 1, \omega 1)$ is the nonlinear

transfer function relating the phasor $Ids(3\omega 1)$ of the nonlinear current source to the corresponding excitation

$$Hds_3(\omega 1,\omega 1,\omega 1)=\frac{Ids(3\omega 1)}{\frac{Vs^3(\omega 1)}{4}}=Hds_{3a}(\omega 1,\omega 1,\omega 1)+Hds_{3b}(\omega 1,\omega 1,\omega 1)+Hds_{3c}(\omega 1,\omega 1,\omega 1). \quad (14)$$

$Hds3(\omega 1,\omega 1,\omega 1)$ has three components: $Hds_{3a}(\omega 1,\omega 1,\omega 1)$ associated to the third-order resistive coefficients, plus $Hds_{3b}(\omega 1,\omega 1,\omega 1)$ and $Hds_{3c}(\omega 1,\omega 1,\omega 1)$ accounting for the second-order resistive combinations of the first-order control voltages and the second-order ones due to both second-order nonlinear currents $Hds_{3b}(\omega 1,\omega 1,\omega 1)$ for $Igs(2\omega 1)$ and $Hds_{3c}(\omega 1,\omega 1,\omega 1)$ for $Ids(2\omega 1)$. They can be computed as in (15)

$$\begin{aligned}Hds_{3a}(\omega 1,\omega 1,\omega 1)&=K_{Vgs}^3(\omega 1)\cdot Gm3+K_{Vgs}^2(\omega 1)\cdot K_{Vds}(\omega 1)\cdot Gm2d+K_{Vgs}(\omega 1)\cdot K_{Vds}^2(\omega 1)\cdot Gmd2+K_{Vds}^3(\omega 1)\cdot Gd3 \quad (15a)\\ Hds_{3b}(\omega 1,\omega 1,\omega 1)&=\{2\cdot K_{Vgs}(\omega 1)\cdot Z_{ggs}(2\omega 1)\cdot Gm2+[K_{Vgs}(\omega 1)\cdot Z_{dgs}(2\omega 1)+K_{Vds}(\omega 1)\cdot Z_{ggs}(2\omega 1)]\cdot Gmd+2\cdot K_{Vds}(\omega 1)\cdot Z_{dgs}(2\omega 1)\cdot Gd2\}\cdot Hgs_2(\omega 1,\omega 1) \quad (15b)\\ Hds_{3c}(\omega 1,\omega 1,\omega 1)&=\{2\cdot K_{Vgs}(\omega 1)\cdot Z_{gds}(2\omega 1)\cdot Gm2+[K_{Vgs}(\omega 1)\cdot Z_{dds}(2\omega 1)+K_{Vds}(\omega 1)\cdot Z_{gds}(2\omega 1)]\cdot Gmd+2\cdot K_{Vds}(\omega 1)\cdot Z_{dds}(2\omega 1)\cdot Gd2\}\cdot Hds_2(\omega 1,\omega 1). \quad (15c)\end{aligned}$$

$Hgs_{3b}(\omega 1,\omega 1,\omega 1)$ and $Hgs_{3c}(\omega 1,\omega 1,\omega 1)$ are two of the three components in $Hgs_3(\omega 1,\omega 1,\omega 1)$. They analogously consider the second-order reactive combinations of the first-order control voltages and the second-order ones caused by the second-order nonlinear currents $Hgs_{3b}(\omega 1,\omega 1,\omega 1)$ for $Igs(2\omega 1)$ and $Hgs_{3c}(\omega 1,\omega 1,\omega 1)$ for $Ids(2\omega 1)$

$$\begin{aligned}Hgs_{3b}(\omega 1,\omega 1,\omega 1)&=\{j\cdot 6\cdot \omega 1\cdot K_{Vgs}(\omega 1)\cdot Z_{ggs}(2\omega 1)\cdot Cgs2\}\cdot Hgs_2(\omega 1,\omega 1) \quad (16a)\\ Hgs_{3c}(\omega 1,\omega 1,\omega 1)&=\{j\cdot 6\cdot \omega 1\cdot K_{Vgs}(\omega 1)\cdot Z_{gds}(2\omega 1)\cdot Cgs2\}\cdot Hds_2(\omega 1,\omega 1) \quad (16b)\end{aligned}$$

$Hgs_2(\omega 1,\omega 1)$ is the second-order nonlinear transfer function relating the phasor $Igs(2\omega 1)$ of this nonlinear current source to the corresponding excitation, a function that can be easily computed once we extracted $Cgs2$

$$Hgs_2(\omega 1,\omega 1)=\frac{Igs(2\omega 1)}{\frac{Vs^2(\omega 1)}{2}}=j\cdot 2\cdot \omega 1\cdot K_{Vgs}^2(\omega 1)\cdot Cgs2. \quad (17)$$

$K_{Isgs}(3\omega 1)$ and $K_{Isds}(3\omega 1)$ are obtained from (12) with $n=3$, while $Z_{ggs}(2\omega 1)$, $Z_{gds}(2\omega 1)$, $Z_{dgs}(2\omega 1)$, and $Z_{dds}(2\omega 1)$ can be calculated with linear analysis for the second-order circuit, as shown in (18), at the bottom of this page, with $n=2$.

The unknown phases $\alpha_2(\omega 1,\omega 1)$ and $\alpha_3(\omega 1,\omega 1,\omega 1)$ can be obtained taking into account that $Cgs2$ and $Cgs3$ in (9) and (13) are real magnitudes. There are a couple of possible values in each case, but the variation of the coefficient of previous order with $Vgso$ give us the clue for selecting the proper one. There is a pattern, just as it happens with the Ids derivatives, for this selection; thus, once we have made a first consequent extraction, it is quite easy to reproduce the results for other FET's. The above expressions seem to be complex at a first glance; however, they are very simple and direct—neither iterative, nor time-consuming—two significant advantages of Volterra-series analysis.

III. Experimental Derivatives Extraction and Usually Adopted Closed -Form Models Performance

The proposed test setup and the extraction procedure have been recently employed to characterize different FET devices in their saturated region. The extracted $Cgs2$ and $Cgs3$ terms for a very typical NE72084 MESFET are shown in Fig. 4(b)–(c) for bias voltages : $Vdso=3V$ and $-3<Vgso<0V$. It can be appreciated that $Cgs2\approx 0.5*dCgs1/dVgs$, and $Cgs3\approx 0.33*dCgs2/dVgs$ for the whole $Vgso$ range, thus confirming the self-consistency of the proposed experimental procedure. Standard least squares fitting and successive numeric differentiations of $Cgs1(Vgso)$

$$\begin{bmatrix}Z_{ggs}(n\omega 1) & Z_{gds}(n\omega 1) & Z_{gl}(n\omega 1)\\ Z_{dgs}(n\omega 1) & Z_{dds}(n\omega 1) & Z_{dl}(n\omega 1)\\ Z_{lgs}(n\omega 1) & Z_{lds}(n\omega 1) & Z_{ll}(n\omega 1)\end{bmatrix}=\begin{bmatrix}\left.\frac{Vgs(n\omega 1)}{Igs(n\omega 1)}\right|_{Ids(n\omega 1)=0} & \left.\frac{Vgs(n\omega 1)}{Ids(n\omega 1)}\right|_{Igs(n\omega 1)=0} & Z_{gl}(n\omega 1)\\ \left.\frac{Vds(n\omega 1)}{Igs(n\omega 1)}\right|_{Ids(n\omega 1)=0} & \left.\frac{Vds(n\omega 1)}{Ids(n\omega 1)}\right|_{Igs(n\omega 1)=0} & Z_{dl}(n\omega 1)\\ \left.\frac{Vl(n\omega 1)}{Igs(n\omega 1)}\right|_{Ids(n\omega 1)=0} & \left.\frac{Vl(n\omega 1)}{Ids(n\omega 1)}\right|_{Igs(n\omega 1)=0} & Z_{ll}(n\omega 1)\end{bmatrix}=-\begin{bmatrix}Y_{11}(n\omega 1) & Y_{12}(n\omega 1) & Y_{13}(n\omega 1)\\ Y_{21}(n\omega 1) & Y_{22}(n\omega 1) & Y_{23}(n\omega 1)\\ Y_{31}(n\omega 1) & Y_{32}(n\omega 1) & Y_{33}(n\omega 1)\end{bmatrix}^{-1} \quad (18)$$

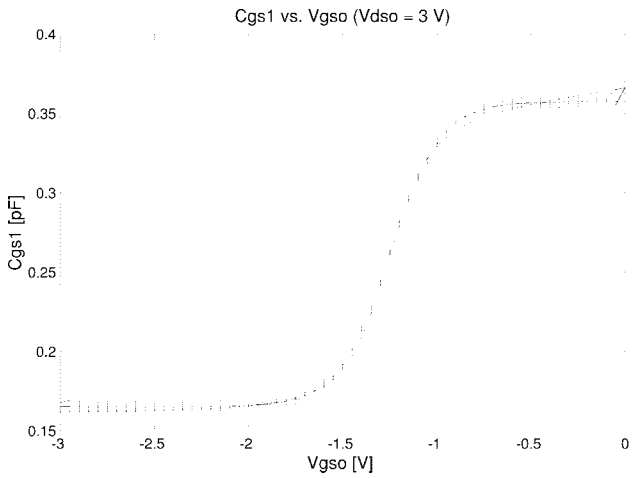

(a)

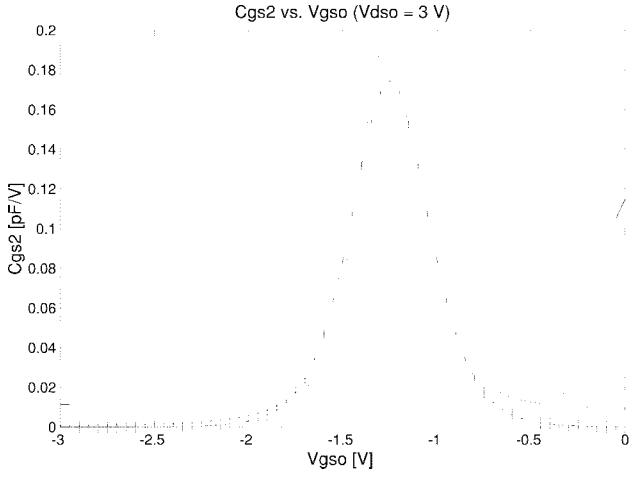

(b)

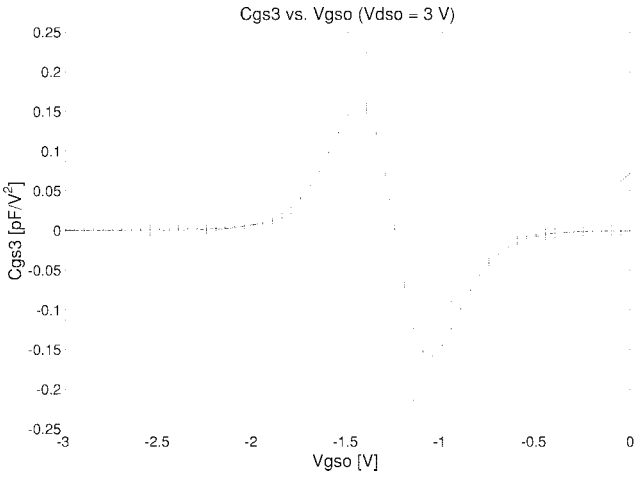

(c)

Fig. 4. Experimental versus model prediction of Cgs Taylor coefficients: (a) $Cgs1$, (b) $Cgs2$, (c) $Cgs3$. [(ooo) = Experimental, (-×-×-) = Statz, (-+-+-) = Scheinberg, (——) = Schottky].

extracted from scattering measurements, the only existing solution up to now [5], are far from producing these smooth results. On the other hand, as we will see further, some of the existing reactive models suffer from high-order derivatives consistency problems.

Moreover, we detected that a careful extraction of the extrinsics, specially Rs, is the key for a successful Cgs characterization, and that some important remarks derived from quasi-linear analysis can give us a complementary tool for validating the different existing techniques for this extraction. One of the most widely employed techniques [13], with the $Rs + Rd$ fourth equation obtained as in [14], but using the real part of Z_{22} from $[S]$ parameters measurements, seems to be the most trustful procedure for the reactive derivatives characterization, as it also seems for the Ids Taylor-terms extraction in the linear region.

The characterization results for $Cgs2$ and $Cgs3$ confirm the exponential nature of the soft MESFET behavior near pinchoff, as it was expected from $Gm2$ and $Gm3$ previous extractions and some common control mechanisms for the depletion region that determine both nonlinearities in these devices. The $Cgs(Vgs)$ dependence is certainly more complex than what a uniform doping profile would suppose; the most commonly used Schottky junction equation does not provide an adequate fit to the gate-to-source-capacitance values extracted from $[S]$ parameters [15], and its second- and third-order derivatives differ a lot from the experimentally extracted ones, as we can appreciate in Fig. 4(b)–(c). The Statz equation [16] for the gate charge, probably one of the best solutions, improve the fitting $Cgs1$ results and provide a much better performance for the higher derivatives shape versus $Vgso$, although the third derivative lobes are symmetric and the $Cgs3$ null in the high-gain region (an interesting bias point for this nonlinearity slightly to the left from the $Gm3$ sweet spot) is not always properly described. The Scheinberg equation [17], of exponential nature, besides providing greater fitting accuracy in the linear and saturated regions, has acceptable higher derivatives with the same particular problems in the high-gain-region behavior than [16]. We will include the derivatives of the Schottky equation in the C/I ratio calculations of Section IV in order to quantify the effects of the mentioned differences in the IMD role of this nonlinearity.

IV. Nonlinear Cgs Role on C/I Distortion Ratio

Fig. 5 shows the evolution of the carrier-to-third-order intermodulation ratio (C/I) for two-tone excitation (something more revealing than the single-tone case) versus frequency and gate bias with a simple 50-Ω load, for Cgs linear, nonlinear, and the Schottky equation. The tones were 10-MHz apart, with an input power (Pin) of -10 dBm each. We can notice the growing significance of the $Cgs(Vgs)$ IMD role when the frequency increases in the microwave region and certain bias shift of the mentioned sweet spot (the relevant peak for $Vgso$ in the high-gain region, useful for low-distortion designs). The interesting frequency behavior experimented by the sweet spot is highlighted by a solid line.

The observed differences in C/I between Fig. 5(a) and (b) can go up to 20 dB in the microwave range, which is mainly due to a relative stronger contribution of the $2\omega 1 - \omega 2$ load current component caused by the reactive nonlinearity. However, there is not appreciable Cgs contribution, as we could expect, in the low-frequency region; thus confirming

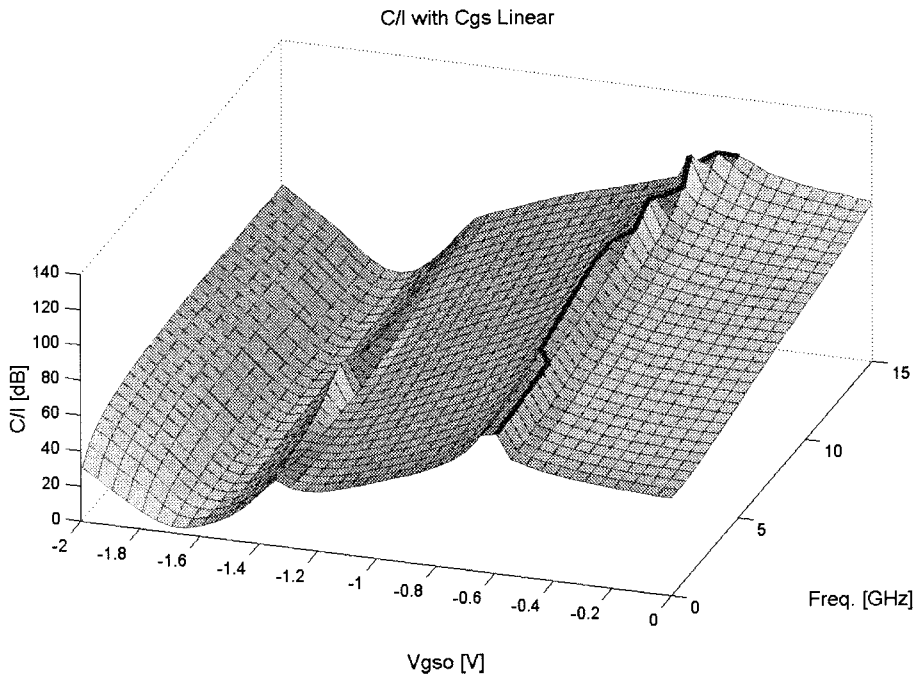

(a)

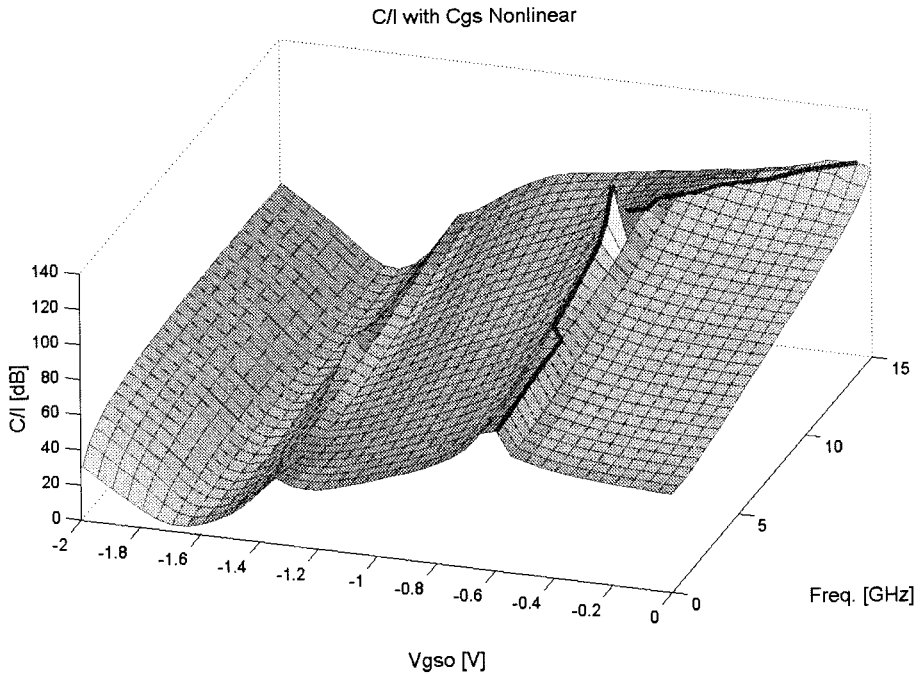

(b)

Fig. 5. Two-tone excitation C/I versus bias and frequency. (a) Cgs linear. (b) Cgs nonlinear.

the validity of the Ids high-order derivatives' extraction methodology at a few hundred megahertz [2]–[4].

The small-signal C/I prediction with the $Cgs(Vgs)$ Schottky equation in Fig. 5(c) differs from the results shown in Fig. 5(b), especially for high frequencies because of its poor $Cgs2$ and $Cgs3$ reproduction.

As was considered in [12], the reactive nonlinearity compensation—see maximum point in Fig 5(b)—would be significant and valuable for narrow-band applications around the optimum bias points, where an accurate $Cgs(Vgs)$ characterization, as the one we propose, could give us the possibility of predicting such situation; but its high selectivity could also limit its extension for some important current wide-band applications.

The C/I load–pull contours, for two-tone excitation at 10 and 10.01 GHz with $Pin = -10$ dBm per tone, using the complete $Ids(Vgs, Vds)$ expansion and Cgs either linear [Fig. 6(a)] or nonlinear [Fig. 6(b)] give us some further insight into its IMD role with load impedance control. We have swept the load reflection coefficient for the first band $ZL(\omega 1) = ZL(\omega 2) = ZL(2\omega 1 - \omega 2) = ZL(2\omega 2 - \omega 1)$, we have assured

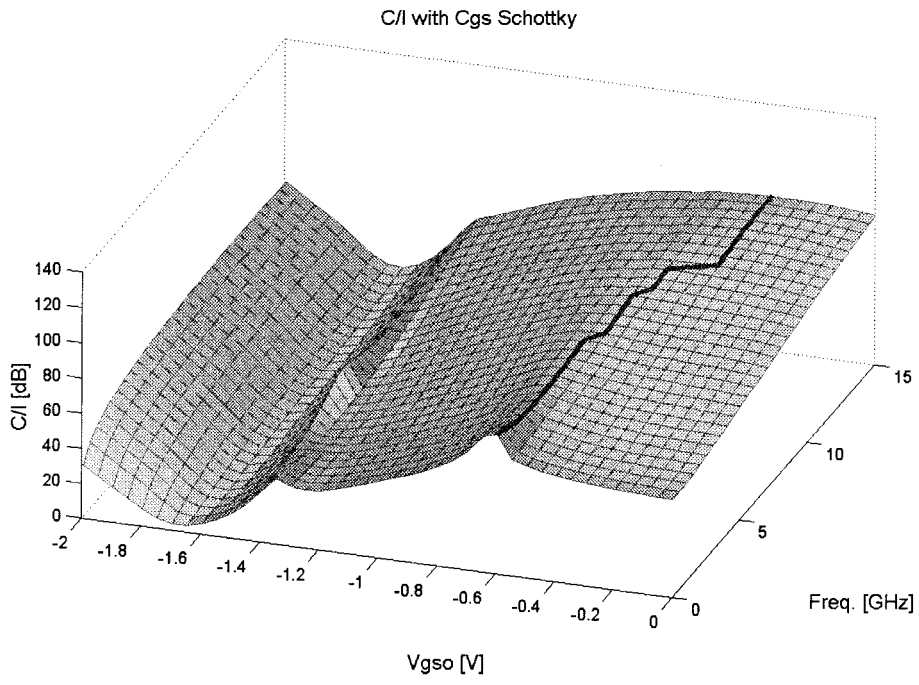

(c)

Fig. 5. *(Continued.)* Two-tone excitation C/I versus bias and frequency. (c) Schottky equation. Solid line represents sweet-spot evolution.

stability, and we have corrected the source available power according to the transistor input reflection coefficient, in order to guarantee a constant input power at the device terminals as it is usually made in measurements of this kind. The bias point: $Vgso = -0.2$ V and $Vdso = 3$ V was employed for the remaining analysis. Output power $(Pout)$ contours (-2, -5, -8, and -10 dBm) are also shown.

Having placed a port at the load in Section II results in a great help for these sections calculations. K_{Vl}, Z_{lgs}, and Z_{lds} lets us now obtain the Vl phasors at the frequencies of our interest, and the corresponding Il phasors and powers in a simple and direct way. We have considered the $Ids(Vgs, Vds)$ complete expansion due to the contribution of the cross terms on IMD cancellations for certain load conditions, as it has been considered in [4]–[5].

The differences, imposed by $Cgs2$ and $Cgs3$ terms, are not precisely in the load–pull C/I contours' general shape, but in certain rotation of the contours, smoother cancellations, and an important shift of the optimum load point for high C/I and high-output-power tradeoffs, a valuable criteria for designing low-distortion small-signal class-A amplifiers. The C/I load–pull prediction with the Schottky equation in Fig 6(c) confirms its inaccuracy for IMD analysis purposes.

Besides showing the typical load–pull contours, we present in Fig. 7 an interesting diagram proposed some years ago by Sechi [18], which presents the output power and C/I evolution versus $|\Gamma|$, where Γ represents the reflection-coefficient vector from the maximum output power point to the points of either the highest C/I (represented for the positive Γ values) or the lowest C/I (represented for the negative Γ values) in each output power contour. The obtained behavior is similar to the one reported, although the points' position differs from a straight line, Fig. 7(b), when we move apart from the optimum power point because of a more complex characterization. This diagram, as well as the C/I range dependence with output power (CIR diagram) in Fig. 8, representing in a simple way the C/I range we can obtain for a given output power, result very didactic for evaluating the nonlinear $Cgs(Vgs)$ role on low-distortion designing criteria.

The point of high C/I at $ZL = 91.58 + j8.78\Omega$, previously represented by "$*$" in Fig. 6(b), corresponds to an output power about 1 dB below the maximum value, a good design tradeoff for a low-distortion amplifier. With Cgs linear, the optimum selection would have differed.

V. Second-Band Source–Pull and Load–Pull C/I Control

In this section, we intend to evaluate the influence that second-order frequencies' terminating impedances $Z(2\omega 1) = Z(\omega 1 + \omega 2) = Z(2\omega 2)$ and $Z(\omega 2 - \omega 1)$ at gate and drain terminals could have on the C/I behavior for a small-signal class-A amplifier employing a MESFET whose reactive and resistive derivatives were experimentally characterized. We selected the load impedance at the first band for the maximum output power, the "$\circ$" point in Fig. 6(b), and the source impedance for input matching, following a typical power gain design. Then, we varied both second-band source and load impedances to see if the output contribution of the $Hgs2$ second-order nonlinear transfer function for Cgs nonlinearity could introduce an important extra C/I control with respect to the Hds_2 transfer-function role due to Ids nonlinearity. For this typical MESFET, in a small-signal class-A-amplifier application with the referred first-band load conditions, and for the classical two-tone input signal, these terminations result in no practical significance (1 dB or less), validating the

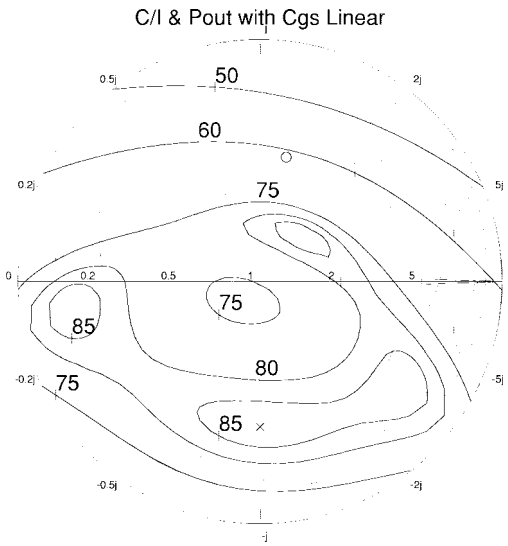

(a)

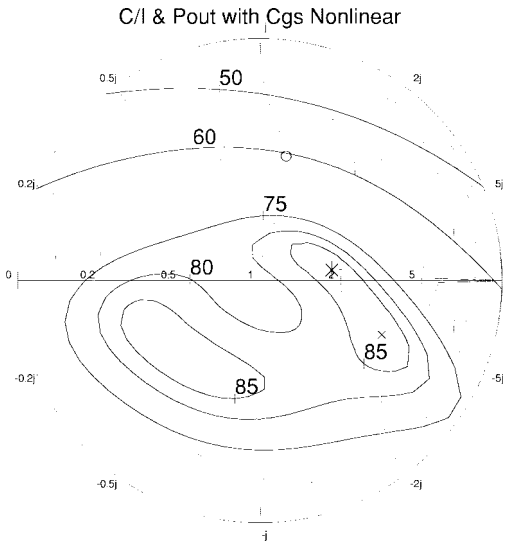

(b)

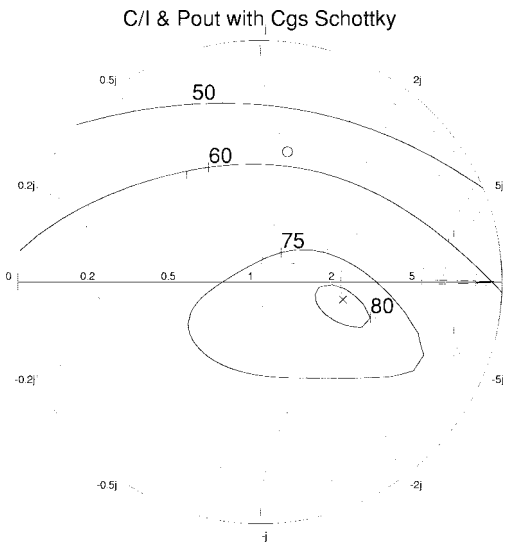

(c)

Fig. 6. C/I (——) in decibels and $Pout$ (- - -) load–pull contours. (a) Cgs linear. (b) Cgs nonlinear. (c) Schottky equation. [(∘) = maximum $Pout$, (×) = maximum C/I, (∗) = design point].

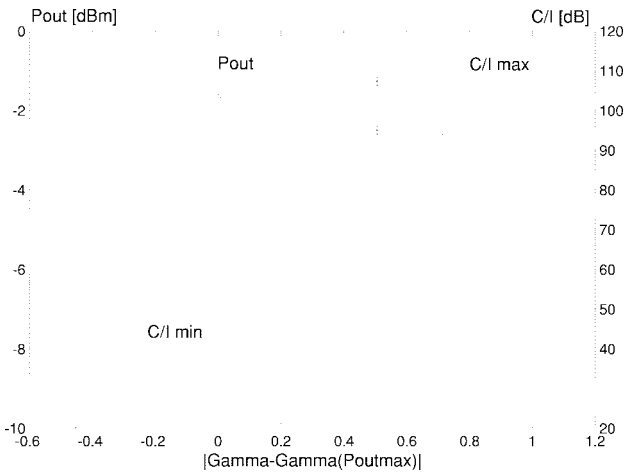

(a)

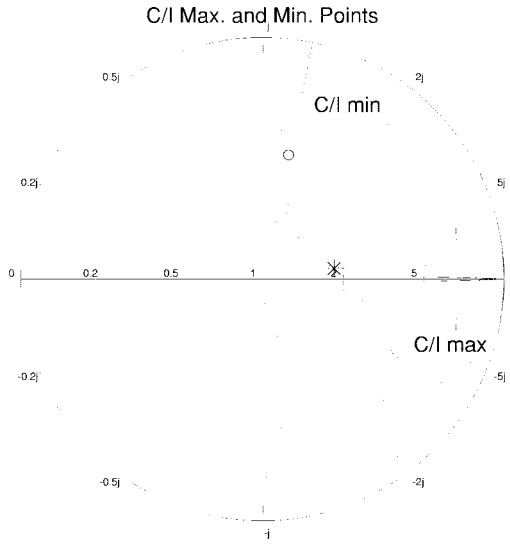

(b)

Fig. 7. Sechi diagrams: (a) C/I (——) and $Pout$ (- - -) versus reflection coefficient. (b) C/I border locations. [(∘∘∘) = maximum, (×××) = minimum, (∗) = design point].

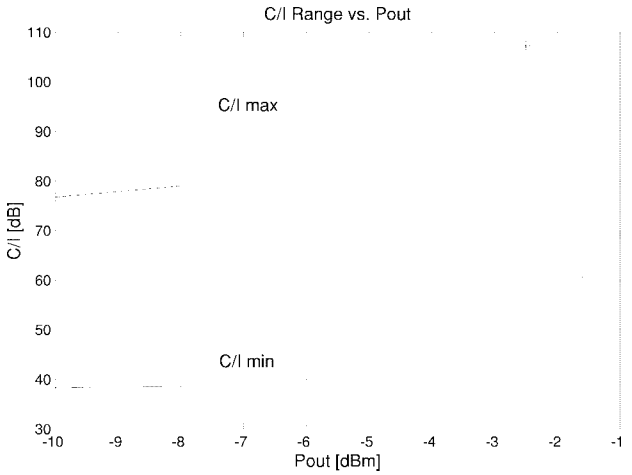

Fig. 8. C/I range versus output power [(-∘-∘-) = maximum, (-×-×-) = minimum].

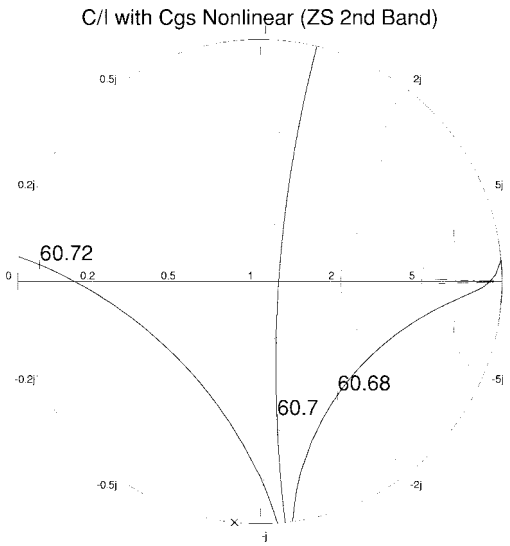

(a)

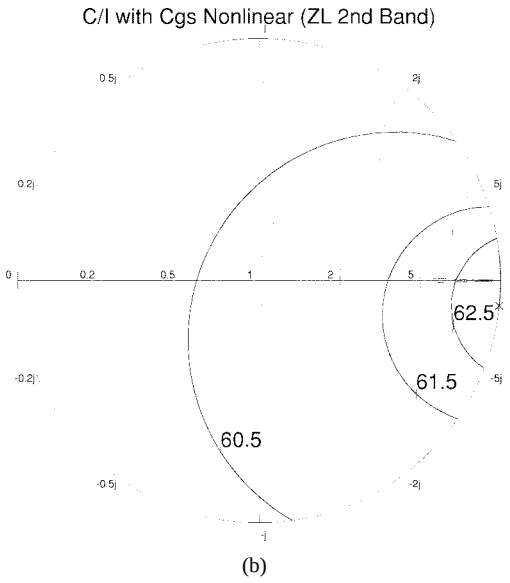

(b)

Fig. 9. C/I [decibels] contours for second-band control. (a) Source–pull. (b) Load–pull [(×) = maximum C/I].

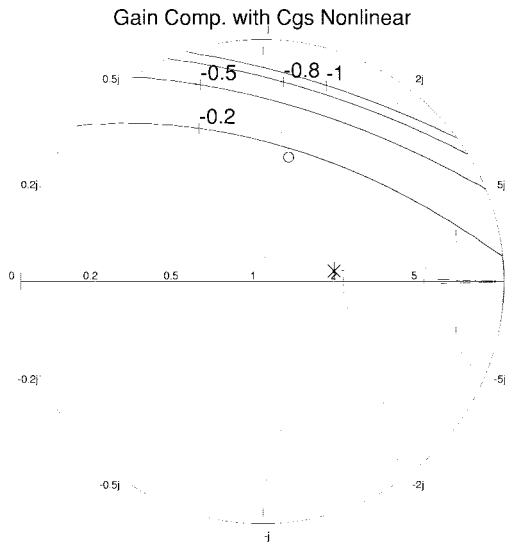

(a)

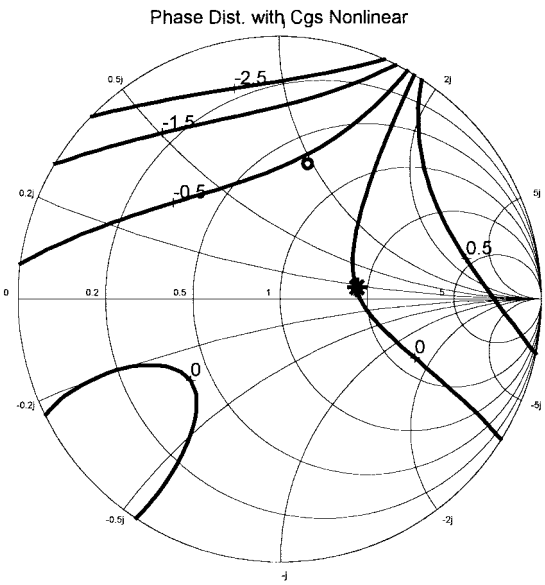

(b)

Fig. 10. Relative distortion vector contours. (a) Gain Compression [decibels]. (b) Phase distortion [°]. [(∘) = maximum $Pout$, (∗) = design point].

predominant contribution of Ids nonlinearity for the second-order components. The supporting computed C/I contours are shown in Fig. 9.

For other conditions, as class-B amplifiers or first-band load conditions where the contributions from third-order terms are small, the second-band impedance control could be more significant.

VI. Nonlinear Cgs Role on Phase Distortion and Gain Compression

Volterra-series analysis up to third order has been proven to be valid [12] for AM/PM conversion, gain saturation, and some other nonlinear related phenomena calculations for input power levels up to approximately the 1-dB compression point, while the device has not been driven into strong saturation. The load–pull contours for phase distortion have been published in a few papers, such as [10], and can be considered in the optimum-load-condition selection.

For a single-tone excitation, once we have characterized the device and numerically computed the nonlinear transfer function $H_3(\omega 1, \omega 1, -\omega 1)$ relating the $Il(\omega 1+\omega 1-\omega 1)$ third-order phasor with the corresponding excitation $Vs^3(\omega 1)/4$, we can easily evaluate both phase distortion and gain compression through the relative distortion vector $D(\omega 1)$ as in [12]

$$D(\omega 1) = 1 + \frac{3}{4} \cdot |V_s(\omega 1)|^2 \cdot \frac{H_3(\omega 1, \omega 1, -\omega 1)}{H_1(\omega 1)}. \qquad (19)$$

The load–pull contours for its magnitude in decibels (gain compression) and its phase in degrees (phase distortion) are shown in Fig. 10 for a single tone at 10 GHz with an input power that drives the device near the small signal regime limits ($Pin = 3$ dBm). The previously selected load condition for high C/I and output power $ZL = 91.58 + j8.78\Omega$ provides an almost null phase distortion supporting our designing criteria.

VII. Conclusions

In this paper, Volterra calculations based on a complete experimental nonlinear characterization, now including the $Cgs(Vgs)$ Taylor-series coefficients extracted for a GaAs MESFET with our proposed test setup, are employed to justify the extent of this reactive nonlinearity increasing role on MESFET IMD performance for high frequencies. Several representative models for this reactive nonlinearity are analyzed for IMD purposes, pointing out their pros and cons. Some variations on the optimum load selection for high C/I and high-output-power tradeoffs due to $Cgs(Vgs)$ derivatives are also considered, as well as their minor role on second-order source and load-distortion control for small-signal class-A amplifiers. Other nonlinear phenomena are also characterized through load–pull contours, giving the possibility of including them in the load condition selection if the phase distortion results are of interest. The suggested characterization procedure is based on the existing techniques for the predominant nonlinearity Ids and intends to complement them in order to have an accurate device characterization for nonlinear distortion purposes. $Cgs(Vgs)$ IMD role for multitone excitation and other important applications in the saturated region, such as gate active mixers, could be also analyzed with the derivatives knowledge and making use of the proper simulation techniques.

Appendix

The previously reported $G2$ and $G3$ Ids derivatives in (A.1) for the transconductance expansion [2], [3], extracted from single-tone low-frequency harmonic measurements at drain side, and the ones in (3) for the complete expansion [4] with two-tone characterization, can be shown to be approximately equivalent for the 50-Ω load condition, giving us the possibility of also extracting $Cgs(Vgs)$ derivatives from the transconductance characterization

$$Ids(Vgs) = Ids(Vgso, Vdso) + Gm1 \cdot vgs + Gds \cdot vds + G2 \cdot vgs^2 + G3 \cdot vgs^3 \quad \text{(A.1)}$$

For extracting $Cgs2$, we would only have to substitute $Hds_2(\omega 1, \omega 1)$ in (9) for (A.2) instead of (10)

$$Hds_2(\omega 1, \omega 1) = \frac{Ids(2\omega 1)}{\frac{Vs^2(\omega 1)}{2}} = K^2_{Vgs}(\omega 1) \cdot G2. \quad \text{(A.2)}$$

In the $Cgs3$ calculation, $Hds_{3a}(\omega 1, \omega 1, \omega 1)$, $Hds_{3b}(\omega 1, \omega 1, \omega 1)$, and $Hds_{3c}(\omega 1, \omega 1, \omega 1)$ in (14) should be analogously substituted for (A.3a–A.3c) in place of (15a–15c)

$$Hds_{3a}(\omega 1, \omega 1, \omega 1) = K^3_{Vgs}(\omega 1) \cdot G3 \quad \text{(A.3a)}$$

$$Hds_{3b}(\omega 1, \omega 1, \omega 1) = \{2 \cdot K_{Vgs}(\omega 1) \cdot Z_{ggs}(2\omega 1) \cdot G2\} \cdot Hgs_2(\omega 1, \omega 1) \quad \text{(A.3b)}$$

$$Hds_{3c}(\omega 1, \omega 1, \omega 1) = \{2 \cdot K_{Vgs}(\omega 1) \cdot Z_{gds}(2\omega 1) \cdot G2\} \cdot Hds_2(\omega 1, \omega 1) \quad \text{(A.3c)}$$

The expected C/I and related nonlinear distortion prediction for 50-Ω load condition would be approximately similar, differing significantly when we move apart from this value, as in the contours analysis.

References

[1] S. A. Maas, "How to model intermodulation distortion," in *IEEE MTT-S Symp. Dig.*, 1991, pp. 149–151.

[2] S. A. Maas and A. Crosmun, "Modeling the gate I/V characteristic of a GaAs MESFET for Volterra-series analysis," *IEEE Trans. Microwave Theory Tech.*, vol. 37, pp. 1134–1136, July 1989.

[3] S. A. Maas and D. Neilson, "Modeling MESFET's for intermodulation analysis of mixers and amplifiers," *IEEE Trans. Microwave Theory Tech.*, vol. 38, pp. 1964–1971, Dec. 1990.

[4] J. Pedro and J. Perez, "Accurate simulation of GaAs MESFET's intermodulation distortion using a new drain-source current model," *IEEE Trans. Microwave Theory Tech.*, vol. 42, pp. 25–33, Jan. 1994.

[5] D. R. Webster, D. G. Haigh, G. Passiopoulos, and A. E. Parker, "Distortion in short channel FET circuits," in *Low-Power HF Microelectronics*, G. Machado, Ed. London, U.K.: Inst. Elect. Eng., 1996, pp. 929–958.

[6] A. Mediavilla, A. Tazón, J. L. García, T. Fernández, J. A. García, J. M. García, C. Navarro, and J. M. Zamanillo, "Dynamic properties and modeling of large signal, thermal, optical, and intermodulation effects in microwave GaAs devices," in *WMC Nonlinear Measuring and Modeling Workshop, IEEE MTT-S Symp.*, 1997.

[7] J. A. Garciá, A. Mediavilla, A. Tazón, J. L. García, and J. C. Pedro, "Accurate characterization procedure of FET's reactive nonlinearities for intermodulation analysis," in *GAAS 97 Symp. Dig.*, 1997, pp. 87–90.

[8] S. Peng, P. J. McCleer, and G. I. Haddad, "Nonlinear models for the intermodulation analysis of FET mixers," *IEEE Trans. Microwave Theory Tech.*, vol. 43, pp. 1037–1045, May 1995.

[9] R. Hajji, F. Beauregard, and F. M. Ghannouchi, "Multitone power and intermodulation load-pull characterization of microwave transistors suitable for linear SSPA's design," *IEEE Trans. Microwave Theory Tech.*, vol. 45, pp. 1093–1099, July 1997.

[10] F. M. Ghannouchi , G. Zhao, and F. Beauregard, "Simultaneous AM–AM/AM–PM distortion measurements of microwave transistors using active load-pull and six-port techniques," *IEEE Trans. Microwave Theory Tech.*, vol. 43, pp. 1584–1588, July 1995.

[11] J. J. Bussgang, L. Ehrman, and J. W. Graham, "Analysis of nonlinear systems with multiple inputs," *Proc. IEEE*, vol. 62, pp. 1088–1119, Aug. 1974.

[12] S. A. Maas, *Nonlinear Microwave Circuits*. Norwood, MA: Artech House, 1988.

[13] G. Dambrine, A. Cappy, F. Heliodore, and E. Playez, "A new method for determining the FET small-signal equivalent circuit," *IEEE Trans. Microwave Theory Tech.*, vol. 36, pp. 1151–1159, July 1988.

[14] H. Fukui, "Determination of the basic device parameters of a GaAs MESFET," *Bell Syst. Tech. J.*, vol. 58, no. 3, pp. 771–795, 1979.

[15] J. Rodriguez, K. Mezher, and M. Al-Daas, "Computationally efficient and accurate capacitance model for the GaAs MESFET for microwave nonlinear circuit design," *IEEE Trans. Computer-Aided Design*, vol. 13, pp. 1489–1497, Dec. 1994.

[16] H. Statz, P. Newman, I. W. Smith, R. A. Pucel, and H. A. Haus, "GaAs FET device and circuit simulation in spice," *IEEE Trans. Electron Devices*, vol. ED-34, pp. 160–169, Feb. 1987.

[17] N. Scheinberg and E. Chisholm, "A capacitance model for GaAs MESFET's," *IEEE J. Solid-State Circuits*, vol. 26, pp. 1467–1470, Oct. 1991.

[18] F. N. Sechi, "Design procedure for high-efficiency linear microwave power amplifiers," *IEEE Trans. Microwave Theory Tech.*, vol. 28, pp. 1157–1163, Nov. 1980.

José Angel García (S'98) was born in Havana, Cuba, in 1966. He graduated (with honors) in Telecommunications Engineering from Instituto Superior Politécnico "José A. Echeverría" (I.S.P.J.A.E.), in 1988, and is currently working toward the Ph.D. degree at the University of Cantabria, Santander, Spain.

From 1988 to 1991, he was a Radio System Engineer at an HF Communication Center, where he designed antennas and RF blocks. In 1991, he was appointed Instructor Professor at the Telecommunications Engineering Department, I.S.P.J.A.E. His main research interests include nonlinear characterization and modeling of active devices, as well as nonlinear-circuit-analysis tools for amplifiers and mixers applications.

Angel Mediavilla Sánchez (M'92) was born in Santander, Spain, in 1955. He graduated (with honors) from the University of Cantabria, Santander, Spain, in 1978 and received the Doctor of Physics degree in 1984.

From 1980 to 1983, he was Ingénieur Stagière at Thomson-CSF, Corbeville, France. He is currently a Professor in the Department of Electronics, University of Cantabria. He possesses wide experience in analysis and optimization of nonlinear microwave active devices and circuits in both hybrid and monolithic technologies. He has participated in Spanish and European projects in nonlinear modeling (Esprit project 6050 MANPOWER) and microwave and millimeter-wave communication circuits and systems (Spanish Project PlanSAT, European Project CABSINET, etc). His current research fields are active microwave circuits, mainly in the area of nonlinear modeling of GaAs devices and their applications in large-signal computer design.

José Carlos Pedro (S'90–M'95) was born in Espinho, Portugal, on March 7, 1962. He received the diploma and doctoral degrees in electronics and telecommunications engineering from University of Aveiro, Aveiro, Portugal, in 1985 and 1993, respectively.

From 1985 to 1993, he was an Assistant Lecturer at the University of Aveiro, then a Professor, and is currently an Associate Professor. He is also a Senior Research Scientist in the Telecommunications Institute. His main scientific interests include active device modeling and the analysis and design of various nonlinear microwave and optoelectronics circuits, in particular, the design of highly linear multicarrier power amplifiers.

Dr. Pedro received the Marconi Young Scientist Award in 1993.

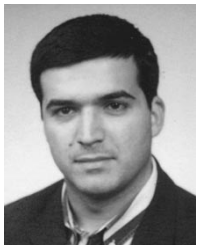

Nuno Borges de Carvalho (S'96) was born in Luanda, Angola, in 1972. He received the diploma degree in electronics and telecommunications engineering from the University of Aveiro, Aveiro, Portugal, in 1995, and is currently working toward the Ph.D. degree.

In 1997 he was appointed Assistant Lecturer at the University of Aveiro. His main research interests include computer-aided design (CAD) for nonlinear circuits and active device modeling and design, mainly for power amplifiers.

Mr. Carvalho is a member of the Portuguese Engineering Association. He received the 1995 University of Aveiro's Best Engineer Student Award and the Portuguese Engineering Association Prize for the 1995 Best Student at the University of Aveiro.

Antonio Tazón Puente (M'92) was born in Santander, Spain, in 1951. He graduated from the University of Cantabria, Santander, Spain, in 1978, and received the Doctor of Physics degree in 1987.

From 1991 to 1995, he was a Professor in the Department of Electronics, University of Cantabria, and since 1996, he has been a Professor in the Department of Communication Engineering. From March to October 1985, and April to July 1986, he carried out research at the IRCOM Department, University of Limoges, France, working in nonlinear modeling and load–pull techniques. He has participated in Spanish and European projects in the nonlinear modeling (Esprit project 6050 MANPOWER) and microwave and millimeter-wave communication circuits and systems (Spanish Project PlanSAT, European Project CABSINET, etc). He has carried out research on analysis and optimization of nonlinear microwave active devices and circuits in both hybrid and monolithic technologies. His current main research interests are active microwave circuits, mainly in the area of linear and large-signal modeling and small-signal intermodulation of GaAs and Si–Ge devices and their applications in nonlinear computer design.

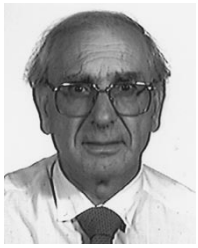

José Luis García (M'74) was born in Zaragoza, Spain, in 1938. He received the M.S.E. degree from the University of Zaragoza, Zaragoza, Spain, in 1964 and the Ph.D. degree from the University of Valladolid, Valladolid, Spain, in 1971.

From 1966 to 1973, he was Associate Professor at the University of Valladolid, where he worked on analog simulation of systems and the generation of pseudorandom signals. In 1973, he became Professor of electronics engineering in the Department of Electronics, University of Cantabria, Santander, Spain, where he has been Dean of the Telecommunications Engineering School and Head of Department. He is currently the Head of the Department of Communications Engineering. He also teaches radiocommunication systems and satellite communications. He has worked in microwave and millimeter-wave systems and components for mobile, radiolinks and satellite communications. His current research interests include broadcasting of digital TV through satellite and SMATV-DTM systems, wireless CDMA-SS for indoor applications, low speed CDMA satellite communications and cellular access to broad-band services, and interactive television at millimeter waves.

Dr. Garcia is member of the Committee of the E-12 professional group of the Institution of Electrical Engineers (IEE), U.K.